Virginia Commonwealth University

VCU Scholars Compass

2018

Material Thermal Property Estimation of Fibrous Insulation: Heat Transfer Modeling and the Continuous Genetic Algorithm

Elora Frye
Virginia Commonwealth University

MATERIAL THERMAL PROPERTY ESTIMATION OF FIBROUS INSULATION: HEAT TRANSFER MODELING AND THE CONTINUOUS GENETIC ALGORITHM

A thesis submitted in partial fulfillment of the requirements for the degree of Master of Science at Virginia Commonwealth University.

by

Elora Frye

Advisor: Rebecca Segal, Ph.D.
Associate Professor
Department of Mathematics and Applied Mathematics

Virginia Commonwealth University
Richmond, Virginia
May 2018

Acknowledgements

I would like to thank my advisor, Dr. Rebecca Segal for encouraging me to pursue writing this thesis as well as being a wonderful mentor. Thank you to Dr. Laura Ellwein-Fix for graciously serving on my committee. Thank you to Dr. Kamran Daryabeigi for his patience, kindness, and reassurance. This work would not be possible without his teaching and encouragement. Lastly, I would like to thank my family and friends for their love and support.

Table of Contents

List of Figures

List of Tables

Abstract

MATERIAL THERMAL PROPERTY ESTIMATION OF FIBROUS INSULATION: HEAT TRANSFER MODELING AND THE CONTINUOUS GENETIC ALGORITHM

By Elora Frye, B.S.

A thesis submitted in partial fulfillment of the requirements for the degree of Master of Science at Virginia Commonwealth University.

Virginia Commonwealth University, 2018

Major Director: Rebecca Segal, Ph.D., Associate Professor, Department of Mathematics and Applied Mathematics

Material thermal properties are highly sought after to better understand the performance of a material under particular conditions. As new materials are created, their physical properties will determine their performance for various applications. These properties have been estimated using many techniques including experimental testing, numerical modeling, and a combination of both. Existing methods can be time consuming, thus, a time-efficient and precise method to estimate these thermal properties was desired. A one-dimensional finite difference numerical model was developed to replicate the heat transfer through an experimental apparatus. A combination of this numerical model and the Continuous Genetic Algorithm optimization technique was used to estimate material thermal properties of fibrous insulation from test data. The focus of this work was to predict these material thermal properties for an Alumina Paper that is commonly used in aerospace applications. The background, methodology, and results are discussed.

Chapter 1

Introduction and Overview

1.1   Introduction

Material thermal properties are highly sought after to predict reliability and performance of a material when exposed to a change in temperature. These thermal properties are known as thermal conductivity and specific heat capacity. Thermal conductivity tells how well a material conducts heat. A material with a high thermal conductivity is known as a good conductor. Many metals, such as Aluminum, are good conductors. A material with a low thermal conductivity is known as an insulator. For example, insulation is used in walls of homes to keep the heat from leaving or entering. Insulation has many applications, including refrigerators, clothes, automobiles, and aerospace applications. An example of an aerospace application is the use of insulation in thermal protection systems (TPS). These structures are built to protect space flight vehicles from the large thermal loads experienced during entry into a planet's atmosphere. The material thermal properties of these insulation are highly sought after in order to predict material reliability and performance during use in a TPS. Fibrous insulation are commonly used as they weigh less than other insulation and weight is a concern in aerospace applications. When new insulation materials are created for these applications, their material thermal properties

are needed to determine if the new material will be successful in the particular application.

1.2   Motivation and Goals

Thermal material properties can vary with temperature and pressure, thus, determining their values can be a daunting task. There have been many techniques used to estimate these properties, including experimental methods, numerical methods, and combinations of the two. Currently, these methods can be quite time consuming. The goal of this work was to validate methodology for quickly and accurately estimating these material thermal properties as functions of temperature and pressure. This was done using a transient thermal testing apparatus to collect temperature data within the material when exposed to large thermal loads. A numerical model was built to replicate the heat transfer through the material which results in computed temperature data. The material thermal property values are then estimated using an optimization method, the Continuous Genetic Algorithm (CGA), to estimate coefficients of a functional form for the material thermal property. This is known as an inverse heat transfer problem. The methodology and the application is discussed, as well as the results of estimating the thermal properties of a common fibrous insulation used in aerospace applications, Alumina Paper (APA).

1.3   Overview

In this research, methodology to predict material thermal properties by solving the inverse heat transfer problem was examined. The goal was to estimate the thermal properties for a fibrous insulation APA for which the values are known and validated. This allows for comparison of the results to the known values to verify the process.

Chapter 2 discusses the background of heat transfer including the derivation of the conduction heat transfer equation. The parameters in the heat transfer equation, which are known as material thermal properties, are also introduced. The current, most common methods of estimating these properties are also summarized in Chapter 2. In Chapter 3, the direct and inverse heat transfer problems are presented. This includes how heat transfer is modeled in an experimental apparatus by a finite difference scheme known as the direct heat transfer problem. The CGA, for the inverse heat transfer problem is introduced in Chapter 3. After discussing this methodology in a general context, explanation of the application of the technique to actual temperature data from a transient thermal testing apparatus is presented in Chapter 4. This includes discussion of components within the setup and the numerical model built to replicate the one-dimensional heat transfer within the apparatus. In Chapter 5, the results of the application for three tests are presented and discussed. The concluding remarks and future research are discussed in Chapter 6.

Chapter 2

Heat Transfer Background

The theory of heat transfer stems from the field of thermodynamics which studies heat as it relates to work and energy. Heat is a form of energy that can be transferred between two objects or within an object. This transfer of heat energy is known as heat transfer and has three main forms: conduction, convection, and radiation. Conductive heat transfer is the movement of energetic particles to less energetic particles. This can take place in solids, liquids, or gases. Faster moving particles have larger heat energy and transfer heat energy to other slower moving particles by bumping into them and in turn making them move faster. Convection is the transfer of heat between a solid surface and the adjacent moving liquid or gas.

A standard definition of radiative heat transfer, as defined from [1] is as follows:

Radiative heat transfer is the energy emitted by matter in the form of electromagnetic waves (or photons) as a result of the changes in the electronic configurations of the atoms or molecules. (p. 27)

This type of heat transfer does not require the two mediums to be adjacent [1]. Any body above zero Kelvin emits thermal radiation.

4

2.1 Heat Transfer Equation

Physical phenomena, which vary in time and space, can be modeled by partial differential equations (PDE), and are often derived from basic physical principles. Most heat transfer textbooks use these three basic principles and a simple example to derive the heat conduction PDE. The first principle is the equation for heat energy, $H_t = c_p m T(x,t)$. The parameter, $c_p \left(\frac{Energy}{Mass \cdot Temperature} \right)$, represents the specific heat of the material, m, represents the mass, and $T(x,t)$ represents the temperature at position x and time t. The second principle is Fourier's Law of Heat Conduction. This says the rate of heat flow is directly proportional to the surface area, A, thermal conductivity, $k \left(\frac{Power}{Length \cdot Temperature} \right)$, and negative temperature gradient through the material. In one-dimensional heat transfer, this is the derivative of temperature with respect to position, x, given by, $Q = -kA \frac{\partial T(x,t)}{\partial x}$ and is known as the heat transfer rate. The third and final principle used is Conservation of Energy. To describe this concept, consider a uniform rod with length, L as seen in Figure 2.1 below.
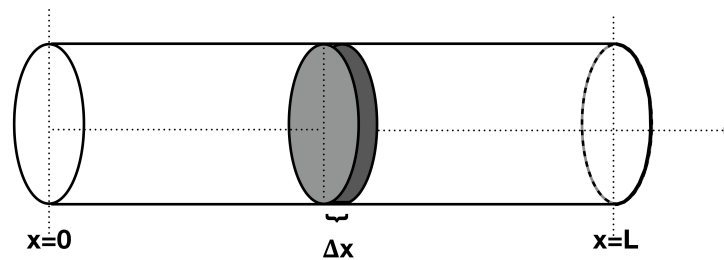
Figure 2.1: Uniform Rod with Length, L

It is assumed that the density, ρ, specific heat at a constant pressure, c_p, thermal conductivity, k, and lateral surface area, A, are all constant. It is also assumed that only one end of the rod is exposed to heat and the other end is kept at a constant temperature. Consider a thin slice of the rod, as seen in dark gray above, with a length Δx. Let $T(x,t)$ be the temperature at the left side of the slice and let $T(x + \Delta x, t)$ be the temperature on the right side of the slice at time, t. Conservation of energy says that the difference between

5

the energy that enters the slice from the left and the energy that leaves that slice from the right, must equal the energy stored in the slice. For this example, it is assumed that there is not a heat source within the rod, thus no heat is generated.

$$Energy_{in} - Energy_{out} = Energy_{stored}$$

$Energy_{in}$, $Energy_{out}$, and $Energy_{stored}$ will be represented using the first two principles discussed. From the heat energy equation, the heat energy of the thin slice at time, t, is $H_t = c_p m T(x,t)$. The mass of the material can be represented as volume times density, $m = V\rho$. The volume can be replaced with the cross-sectional surface area multiplied by the the width of the slice, Δx. Thus, the heat energy of the slice at a particular time, t, is $H = c_p \rho A \Delta x T(x,t)$. This is used to denote $Energy_{stored}$ over a particular time, Δt.

$$Energy_{stored} = H_{t+\Delta t} - H_t = c_p \rho A \Delta x T(x, t + \Delta t) - c_p \rho A \Delta x T(x,t)$$

The $Energy_{in}$ and $Energy_{out}$ will be represented by Fourier's Law of Heat Conduction. $Q_x = -kA\Delta t \frac{\partial T(x,t)}{\partial x}$ can represent $Energy_{in}$ at position x, or the heat transfer rate across the disc at position x, and $Energy_{out}$ similarly can be represented by $Q_{x+\Delta x} = -kA\Delta t \frac{\partial T(x+\Delta x,t)}{\partial x}$. Substituting these back into the Conservation of Energy equation the following is achieved:

$$Q_x - Q_{x+\Delta x} = H_{t+\Delta t} - H_t$$

$$\left(-kA\Delta t \frac{\partial T(x,t)}{\partial x}\right) - \left(-kA\Delta t \frac{\partial T(x+\Delta x,t)}{\partial x}\right) = c_p \rho A \Delta x T(x, t + \Delta t) - c_p \rho A \Delta x T(x,t)$$

Dividing both sides by A:

$$\left(-k\Delta t \frac{\partial T(x,t)}{\partial x}\right) - \left(-k\Delta t \frac{\partial T(x+\Delta x,t)}{\partial x}\right) = c_p \rho \Delta x T(x,t) - c_p \rho \Delta x T(x, t + \Delta t)$$

Rearranging and dividing both sides by Δx and Δt:

$$k\left(\frac{\dfrac{\partial T(x+\Delta x, t)}{\partial x} - \dfrac{\partial T(x,t)}{\partial x}}{\Delta x}\right) = c_p \rho \left(\frac{T(x,t) - T(x, t+\Delta t)}{\Delta t}\right)$$

Taking the limit as Δx and Δt approach 0:

$$\lim_{\substack{\Delta x \to 0 \\ \Delta t \to 0}} \left[k\left(\frac{\dfrac{\partial T(x+\Delta x, t)}{\partial x} - \dfrac{\partial T(x,t)}{\partial x}}{\Delta x}\right) = c_p \rho \left(\frac{T(x,t) - T(x, t+\Delta t)}{\Delta t}\right) \right]$$

$$\frac{\partial}{\partial x}\left(k\frac{\partial T(x,t)}{\partial x}\right) = c_p \rho \frac{\partial T(x,t)}{\partial t} \tag{2.1}$$

This is the simple partial differential equation that models conductive heat transfer. In the uniform rod example, the thermal conductivity, k, can be factored out of the first partial derivative since it is assumed to be constant. However, if the thermal conductivity is a function of position, time, or temperature, it cannot be factored out. In mediums with high porosity, such as insulations, thermal conductivity does vary with temperature as well as pressure. When using this heat transfer equation to accurately model a particular physical situation, thermal conductivity is represented as a function of temperature and pressure [1].

2.2 Thermal Properties

Thermal properties such as specific heat and thermal conductivity can be difficult to estimate, as they can be functions of many variables such as temperature, pressure, and material characteristics.

2.2.1 Thermal Conductivity

The following definition for thermal conductivity is taken from [1]:

Thermal Conductivity is the rate of heat transfer through a unit thickness of the material per unit area per unit temperature difference. (p. 20)

Some examples of materials with a large thermal conductivity values are metals such as, aluminum, gold, and copper, as well as diamond. Materials with low thermal conductivity include rubber and insulation. This work focuses on heat transfer through fibrous insulation, a material made from fibers that include pores or gaps in between the fibers as seen in Figure 2.2. The thermal conductivity of these types of materials is a combination of the thermal conductivity of the solid (fibers), the thermal conductivity of gas (space between fibers or pores), and the thermal conductivity from radiation. The thermal conductivity of gas varies with pressure, thus the combined thermal conductivity of the insulation varies with temperature and pressure. According to Daryabeigi et al. [2], since the thermal conductivity of gas plays a role in the overall thermal conductivity of the porous material, the size of the pores dictate the amount of gas conduction or heat transfer in the fibrous insulation. Scanning Electron Microscope (SEM) images are used to determine the characteristic length (pore size) of the material as seen in Figure 2.2, a SEM image of APA taken at NASA Langley Research Center.

When characterizing the thermal conductivity of fibrous insulation, the fiber size and the pore size must be determined to find the thermal conductivity from gas, solid, and radiation which sum to the total thermal conductivity [2].

$$k_{tot} = k_s + k_g + k_r \tag{2.2}$$

From [2], k_s and k_g can be modeled with a linear terms, where as k_r can be modeled with a cubic term thus when summed, k_{tot} has a cubic form. In the methodology discussed, it is

8
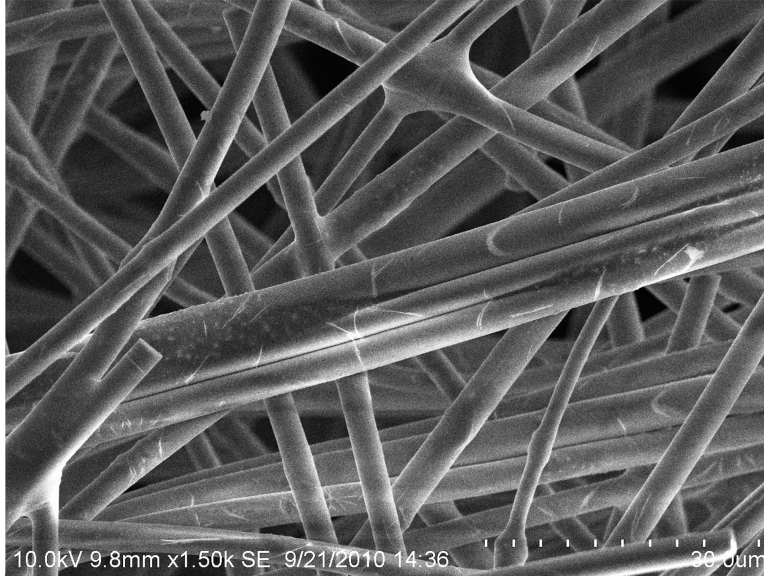
Figure 2.2: Scanning Electron Microscope Image of Alumina Paper Insulation

not required to distinguish between the thermal conductivity of solid, gas, and radiation as the total thermal conductivity is estimated.

2.2.2 Specific Heat

The second thermal property seen in equation 2.1 is specific heat. The following definition for specific heat is taken from [1]:

> *Specific heat is the energy required to raise the temperature of a unit mass of a substance by one degree. (p. 7)*

This is also known as a material's ability to store heat which is why it is used in the $Energy_{stored}$ term. A material's specific heat varies with temperature. Specific heat is denoted c_p.

9

2.3   Estimation Techniques for Thermal Properties

Most previously developed techniques require an experiment to mimic the thermal loads the material is subjected to during these applications. These methods can be limited in temperature range and many require steady-state conditions which can be laborious.

The first experimental method is called the guarded hot plate technique. This technique requires the apparatus to be in steady-state conditions. Reaching these conditions can be very time consuming. This technique has the ability to reach a maximum testing temperature of 1000 degrees Celsius [3]. Another technique used is called the heat flow meter apparatus. This technique is based on the American Society of Testing and Materials (ASTM) Standard C518. A specimen of the material is placed between a cold plate and hot plate with a heat flux transducer. This method also requires waiting for steady-state conditions [4]. The third method is known as the transient radiant setup. This technique requires placement of a cylindrical specimen between two metal plates. The temperature is measured at three locations within the specimen. Numerical techniques are used to model the temperature within the material and a method of least squares is used to match the experimental temperature data to the numerical data [5]. The fourth method is the testing apparatus at NASA Langley Research Center, in Hampton, Virginia. This technique is similar to the heat flow meter apparatus but uses a larger lateral surface area to ensure the heat transfer is one-dimensional. To estimate thermal conductivity, the material is subjected to heat until it has reached the desired temperature. The material is then held at this temperature until it has reached steady-state conditions. From the steady-state data collected, the thermal conductivity values are inferred using the measured heat flux and temperature drop through the material [2]. This process can be laborious as it requires testing at multiple temperatures and various pressures. It is also time consuming to achieve these steady-state conditions. This technique can reach 1500 degrees Celsius.

To estimate specific heat, the standard practice is a Differential Scanning Calorimeter. This device has two heaters connected to a computer. A pan with the sample material is placed on one heater and a empty pan is placed on the the other heater. The computer controls heating of both pans at the same rate. The pan with the sample will require more heat than the empty pan to keep them at the same temperature. The difference in the amount of heat needed from each heater is measured and used to infer specific heat [6]. Out of the two thermal properties, the current method for estimating specific heat is easier to get quick, accurate estimates.

In this work, a combination of ideas for estimating thermal conductivity given above was used. Instead of a steady-state test setup, a transient test setup is used and a numerical model is developed to replicate the temperatures within the apparatus. This transient setup, located at NASA Langley Research Center, was used to collect transient temperature data from an apparatus created to mimic thermal loads the material experiences in flight applications. This data is used in combination with numerical modeling and a CGA optimization technique to infer the material thermal properties. The focus was to use this methodology to estimate the material thermal properties of a well-known fibrous insulation, APA. APA was chosen as its thermal properties are known and validated, [2], which allows for comparison of results. Genetic Algorithms have been used to estimate various aspects of material thermal properties such as in [2] where a genetic algorithm was used to infer specifics about thermal conductivity of radiation from steady-state temperature data. A similar technique has been researched by [7] using a genetic based algorithm to estimate the thermal properties of a material within an infinite cylinder using artificial data. To the author's knowledge, this type of methodology has not been applied to transient temperature data of fibrous insulation and validated with results.

Chapter 3

Direct and Inverse Heat Transfer Problem

Equation 2.1 can be solved analytically if the parameters thermal conductivity, k, specific heat, c_p, and density, ρ, are all assumed to be constant. As discussed, these properties can vary with temperature thus in a realistic model, these would not be constant. To solve a more comprehensive model, numerical methods are used to approximate the solution. Given an initial condition, boundary conditions, and material properties, a finite difference scheme can solve for the temperatures throughout the material by approximating the heat conduction partial differential equation.

3.1   Boundary Conditions

In order to solve Equation 2.1 either numerically or analytically, boundary conditions are needed. This gives information about the PDE at the boundary of the domain. When discussing boundary conditions for heat transfer, there are hot side boundary conditions and cold side boundary conditions. Hot side refers to where the heat is present and cold side refers to the opposite side towards where the heat is moving. There are two main

12

types of possible boundary conditions, Dirichlet and Neumann. A Dirichlet boundary condition specifies the value of the solution on the boundary. This can be a constant number or can vary with time. A Neumann boundary condition specifies the value of the directional derivative to the boundary. A common boundary condition used as the cold side boundary is a zero heat flux. This is known as adiabatic and implies there is no heat leaving the material. In the numerical models discussed, Dirichlet boundary conditions as a specified temperature are used.

3.2   Direct Heat Transfer Problem

Finite difference methods are applied by replacing derivatives in the equation by differences. To begin, the domain in question is discretized into a finite number of nodes. Take an arbitrary set of nodes within a domain as seen in Figure 3.2. The nodes represent locations in the material and the temperatures at these locations are desired.
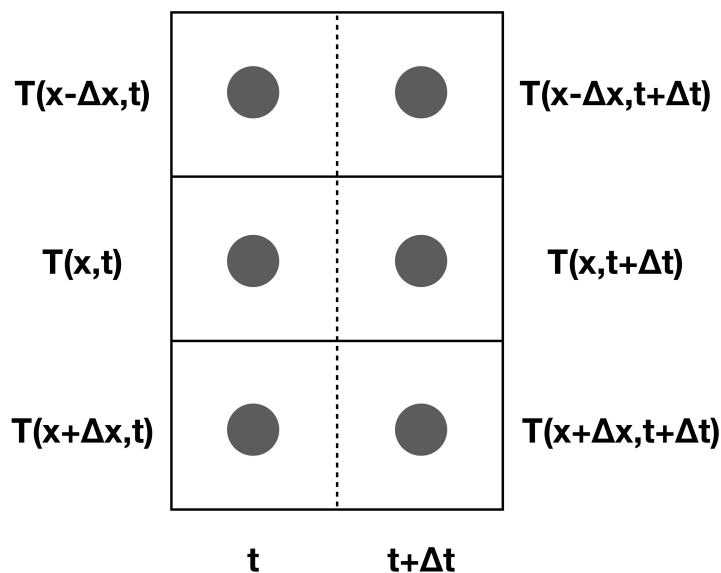
Figure 3.1: Example Discretization for time t and $t + \Delta t$

13

3.2.1   Finite Difference Method

The heat conduction PDE was derived using an Energy Balance as discussed in Chapter 2. To model this PDE numerically, the same technique is used. Let $T_{i,j}$ be the temperature at location i at time j.

First, the time derivative will be approximated as an $Energy_{stored}$ term by finding the temperature difference between the center node from the current and previous time step. Since specific heat varies with temperature, the specific heat function is evaluated at the temperature from the previous time step. Let $c_{p_{i,j}}$ denote the specific heat function evaluated at $T_{i,j}$, $c_{p_{i,j}} = c_p\Big(T_{i,j}\Big)$. Thus, the $Energy_{stored}$ term is as given below:

$$Energy_{stored} = c_{p_{x,t}}\rho\Delta x\left(\frac{T_{x,t+\Delta t} - T_{x,t}}{\Delta t}\right) \tag{3.1}$$

To approximate the spacial temperature derivative, the difference between $Energy_{in}$ and $Energy_{out}$ will be calculated at the previous time step and current time step. For $Energy_{in}$, the temperature difference between nodes $T_{x-\Delta x,t}$ and $T_{x,t}$ and the temperature difference between nodes $T_{x-\Delta x,t+\Delta t}$ and $T_{x,t+\Delta t}$ are found and averaged. The thermal conductivity function is evaluated for each temperature difference at the previous time step. Let $k_i, j = k\Big(\frac{T_{i,j}-T_{i-1,j}}{\Delta x}\Big)$. The $Energy_{in}$ for the example discretized domain is:

$$Energy_{in} = k_{x,t-\Delta t}\left(\frac{T_{x,t} - T_{x-\Delta x,t}}{2\Delta x}\right) + k_{x,t}\left(\frac{T_{x,t+\Delta t} - T_{x-\Delta x,t+\Delta t}}{2\Delta x}\right)$$

Similarly for the $Energy_{out}$ term.

$$Energy_{out} = k_{x+\Delta x,t-\Delta t}\left(\frac{T_{x+\Delta x,t} - T_{x,t}}{2\Delta x}\right) + k_{x+\Delta x,t}\left(\frac{T_{x+\Delta x,t+\Delta t} - T_{x,t+\Delta t}}{2\Delta x}\right)$$

Combining the aforementioned approximation results in:
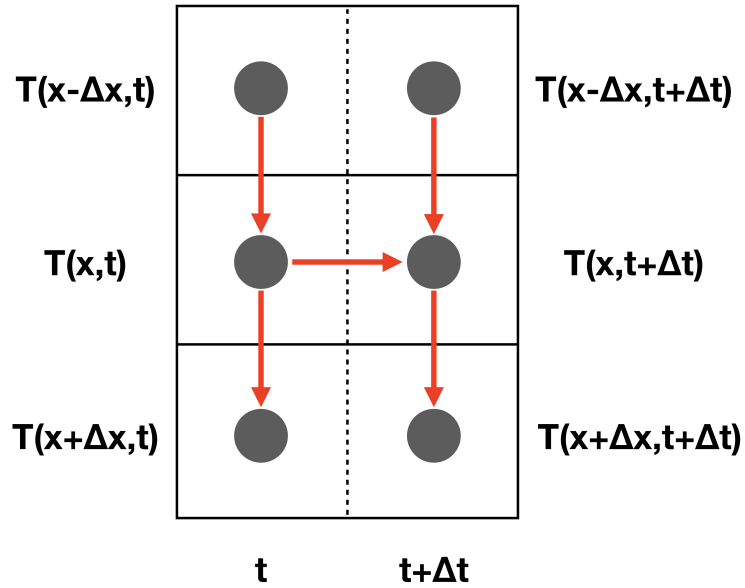
Figure 3.2: Conservation of Energy

$$Energy_{in} - Energy_{out} = Energy_{stored}$$

$$c_{p_{x,t}}\rho\Delta x\left(\frac{T_{x,t+\Delta t} - T_{x,t}}{\Delta t}\right) = k_{x,t-\Delta t}\left(\frac{T_{x,t} - T_{x-\Delta x,t}}{2\Delta x}\right) + k_{x,t}\left(\frac{T_{x,t+\Delta t} - T_{x-\Delta x,t+\Delta t}}{2\Delta x}\right)$$
$$- k_{x+\Delta x,t-\Delta t}\left(\frac{T_{x+\Delta x,t} - T_{x,t}}{2\Delta x}\right) - k_{x+\Delta x,t}\left(\frac{T_{x+\Delta x,t+\Delta t} - T_{x,t+\Delta t}}{2\Delta x}\right)$$

In this equation, there are three unknowns $T_{x-\Delta x,t+\Delta t}$, $T_{x,t+\Delta t}$, and $T_{x+\Delta x,t+\Delta t}$, seen in red above. Thus, if the domain has n nodes, the result is a tridiagonal system of equations as seen in 3.2. This is known as the Crank Nicolson Method. Notice that the system includes the temperatures from nodal positions 2 to $n-1$. This is due to known temperatures at location 1 and n from the specified temperature boundary conditions.

$$\begin{bmatrix} b_2 & c_2 & 0 & 0 & \ldots & 0 \\ a_3 & b_3 & c_3 & 0 & \ldots & 0 \\ 0 & a_4 & b_4 & c_4 & \ldots & 0 \\ \vdots & \ddots & \ddots & \ddots & \ddots & \vdots \\ 0 & \ldots & a_{n-3} & b_{n-3} & c_{n-3} & 0 \\ 0 & 0 & \ldots & a_{n-2} & b_{n-2} & c_{n-2} \\ 0 & 0 & \ldots & 0 & a_{n-1} & b_{n-1} \end{bmatrix} \begin{bmatrix} T_{2,j} \\ T_{3,j} \\ T_{4,j} \\ \vdots \\ T_{n-3,j} \\ T_{n-2,j} \\ T_{n-1,j} \end{bmatrix} = \begin{bmatrix} R_2 \\ R_3 \\ R_4 \\ \vdots \\ R_{n-3} \\ R_{n-2} \\ R_{n-1} \end{bmatrix} \qquad (3.2)$$

$$a_i = -\frac{k_{i-1,j-1}}{2\Delta x}, b_i = \frac{\rho c_{p_{i,j-1}}\Delta x}{\Delta t} + \frac{k_{i-1,j-1}}{2\Delta x} + \frac{k_{i,j-1}}{2\Delta x}, \text{ and } c_i = -\frac{k_{i,j-1}}{2\Delta x}$$

The right hand side for $i = 3$ to $i = n-2$ is:

$$R_i = T_{i,j-1}\Big[\frac{\rho c_{p_{i,j-1}}\Delta x}{\Delta t} - \frac{k_{i-1,j-1}}{2\Delta x} - \frac{k_{i,j-1}}{2\Delta x}\Big] + T_{i-1,j-1}\Big[\frac{k_{i-1,j-1}}{2\Delta x}\Big] + T_{i+1,j-1}\Big[\frac{k_{i,j-1}}{2\Delta x}\Big]$$

R_2 and R_{n-1} have an extra term from the boundary conditions as the temperatures on the boundary are known for the next time:

$$R_2 = T_{2,j-1}\Big[\frac{\rho c_{p_{2,j-1}}\Delta x}{\Delta t} - \frac{k_{1,j-1}}{2\Delta x} - \frac{k_{2,j-1}}{2\Delta x}\Big] + T_{1,j-1}\Big[\frac{k_{1,j-1}}{2\Delta x}\Big] + T_{3,j-1}\Big[\frac{k_{2,j-1}}{2\Delta x}\Big] + T_{1,j}\Big[\frac{k_{2,j-1}}{2\Delta x}\Big]$$

$$R_{n-1} = T_{n-1,j-1}\Big[\frac{\rho c_{p_{n-1,j-1}}\Delta x}{\Delta t} - \frac{k_{n-2,j-1}}{2\Delta x} - \frac{k_{n-1,j-1}}{2\Delta x}\Big] + T_{n-2,j-1}\Big[\frac{k_{n-2,j-1}}{2\Delta x}\Big] + T_{n,j-1}\Big[\frac{k_{n-1,j-1}}{2\Delta x}\Big] + T_{n,j}\Big[\frac{k_{n-1,j-1}}{2\Delta x}\Big]$$

3.2.2 Thomas Algorithm

Various system solvers can be used to solve the system for the temperatures of the nodal locations at time $t + \Delta t$. In this research, the Thomas algorithm was used to solve this tridiagonal system as it can improve computational time compared to general solvers. Suppose the matrix has the tridiagonal form as given in Equation 3.2. The Thomas

Algorithm for the tridiagonal system is given below [9].

1. Replace c_i's and R_i's with:

$$\tilde{c}_i = \begin{cases} \dfrac{c_i}{b_i} & i = 2 \\[2ex] \dfrac{c_i}{b_i - a_i \tilde{c}_i} & i = 3...n-2 \end{cases}$$

$$\tilde{R}_i = \begin{cases} \dfrac{R_i}{b_i} & i = 2 \\[2ex] \dfrac{R_i - a_i \tilde{R}_{i-1}}{b_i - a_i \tilde{c}_i} & i = 3...n-1 \end{cases}$$

2. Perform back substitution to solve for the temperatures:

$$T_{n-1} = \tilde{R}_{n-1}$$

$$T_i = \tilde{R}_i - \tilde{c}_i T_{i+1} \quad i = n-2, ..., 2$$

3.3   Inverse Heat Transfer Problem

When given temperature data, the inverse heat transfer problem has the goal of solving for an unknown in the model such as material thermal properties, k and c_p. In this application, suppose the temperature in the material is known but one of the parameters, k or c_p is unknown. An optimization technique is used to search the parameter space for the values of one of these thermal properties to be used in the direct model. These values are chosen based on how well they minimize the error between the collected temperature and computed model data. The more that is known about the particular thermal property will reduce the number of parameters that need to be estimated. It is assumed that these properties vary with temperature but that their functional forms are known. The direct

17

model is then solved with the estimated parameter values and the calculated temperatures are compared to measured temperatures from the test data.

There are many optimization techniques that have been used to solve this problem including the Conjugate-Gradient and the Levenberg-Marquardt Methods [10]. These methods are gradient based and can be extremely sensitive to the initial guess. Another inverse heat transfer method is the CGA. CGA allows the user to set ranges for each parameter that the algorithm searches within. All three algorithms were attempted, however the CGA was used as it was the fastest and produced the most reliable results.

3.3.1 Continuous Genetic Algorithm

From Practical Genetic Algorithms by Haupt and Haupt [11], the algorithm searches the parameter space for the set of parameters that best minimizes or maximizes the objective function given. The objective function can change based on the application of the algorithm. The general methodology is discussed below.

- **Initial Population:** To generate the initial population, or first set of possible parameter values, the algorithm creates sets of parameters by randomly selecting numbers, using a uniform distribution. These parameter values are selected from specified ranges. Each set of parameters is a row in the population matrix. Thus the matrix is N_{sets} X N_{par}, where N_{sets} is the number of sets of parameters and N_{par} is the number of parameters.

- **Natural Selection:** After creating the initial population, CGA decides which sets should be used to create offspring. To do this, it determines the sets that do the best at minimizing or maximizing the objective function by evaluating it with each set of parameters. After sorting the sets from best to worst, the algorithm selects the top

18

N_{keep} of the population.

- **Pairing:** To assign pairs that will 'mate,' or create offspring, the algorithm randomly matches sets of parameters from the remaining population that survived from natural selection. These randomly selected pairs will create two offspring in the mating process.
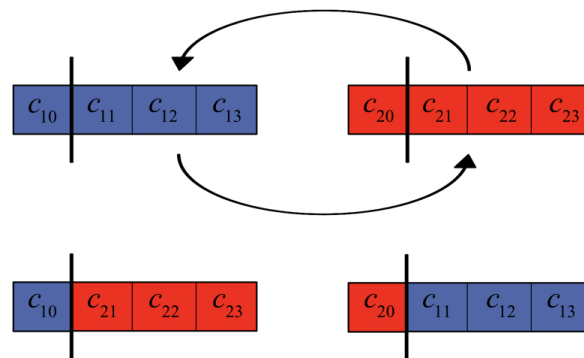
Figure 3.3: Single Point Crossover

- **Mating:** A combination of these parents will create two offspring. To create these offspring, many approaches are possible but for this work, single point crossover was used. An example of single point crossover can be seen in Figure 3.3. A random point in the parameter set is selected as the crossover point then the parameters to the right are swapped. The new combination of parameters are the two offspring of the parents.

- **Mutations:** Haupt and Haupt discusses a known issue with the algorithm. It can converge too quickly to a local minimum or maximum that might not be the global minimum and maximum. To keep CGA from getting trapped, mutations are introduced to add variety to the population. At the beginning, a particular percentage

of the population is chosen to be mutated. To accomplish this mutation, random numbers are selected to determine the row and column of the parameter to be mutated. Once the individual parameters are selected, they are replaced with a random number within the set interval for that parameter.

- **New Population:** If stopping criteria are not satisfied, the new population is used to evaluate the objective function and is again sorted from best to worst. The above process reoccurs until the stopping criteria has been satisfied; either the maximum number of iterations have been used or an objective function has been maximized or minimized to desired tolerance [11].

A combination of the methodology discussed above will be used to numerically model the heat transfer through the materials within a testing apparatus. The Crank Nicolson Method will be used to create the direct heat transfer model and the Thomas Algorithm is used to solve the tridiagonal system. The data from this direct numerical model will be used in the inverse heat transfer problem and will be solved using the CGA. In the next chapter, methodology used for the specific application in this research is discussed.

Chapter 4

Application of Methodology

4.1 Continuous Genetic Algorithm for Heat Transfer

To apply the CGA to the inverse heat transfer problem, the first step was to determine the parameters to be estimated. The initial parameter to be determined was thermal conductivity, k. Next, a functional form of the parameter was determined so its coefficients could be estimated. As discussed in chapter 2, thermal conductivity can be modeled using a cubic polynomial. To estimate this cubic polynomial, the four coefficients, c_0, c_1, c_2, c_3 of the polynomial were found using the CGA.

$$k(T) = c_0 + c_1 T + c_2 T^2 + c_3 T^3 \tag{4.1}$$

Next, a numerical model was built to replicate the test setup. The experiment was then executed and temperature data was collected at various locations within the setup. Using Dirichlet boundary conditions from the recorded temperature data at the boundaries of the domain modeled, the goal was to determine the thermal conductivity of APA by matching the numerical model temperature data to the recorded experimental data inside the test sample. To do this, the CGA estimates the four coefficients for thermal conductivity and uses the estimates as the thermal conductivity within the direct numerical model. To

21
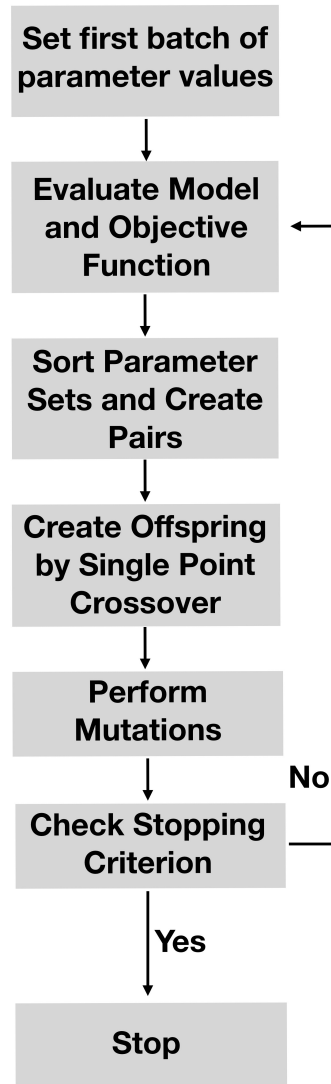
Figure 4.1: The Continuous Genetic Algorithm for Heat Transfer

determine which estimate is best from the original population, the CGA evaluates the objective function given in equation 4.2.

$$z = \sum_{i=1}^{m} \left(\frac{T_n(i) - A(i)}{A(i)} \right)^2 \qquad (4.2)$$

Where, m is the number of time steps, $T_n(i)$ is the computed temperature from the numerical approximation at the nodal location chosen at time i, and $A(i)$ is the measured temperature at the corresponding location in the experiment at time, i. This objective

22

function was chosen to minimize the temperature difference between the model and test data at corresponding nodal locations. The value of this function will be referred to as the associated cost for each run.

The CGA for the heat transfer problem can be seen in Figure 4.1 [11]. It begins by constructing the initial population containing sets of coefficients for the thermal conductivity function. It does this by selecting random numbers between the intervals given for each coefficient and uses these sets individually as the thermal conductivity in the direct model and evaluates the objective function, Equation 4.2. After it has completed this for each set of coefficients, it sorts the objective function values, or cost values from best to worst. The coefficients that were the most successful at minimizing the object function are placed at the top and the sets that did the worst job, placed at the bottom. It then takes the top 50% of the population and randomly pairs the sets together. With these pairs, it creates two offspring by single point crossover, discussed in the last chapter in Figure 3.3. These two new sets of coefficients combine with the original top 50% of the population and create the new population. A percentage of this new population is then mutated to add variety to the possible solutions. The population is then checked against the stopping criterion. If the algorithm has met the maximum number of iterations or if the cost value is below the threshold set, the algorithm terminates. The result is the set of coefficients found that gave the lowest value to the objective function.

4.2   Experiment Setup

In this section, the experimental setup is discussed as well as the one-dimensional numerical model built to replicate the heat transfer through the materials. The temperature data used was collected from a transient thermal testing facility located at NASA Langley
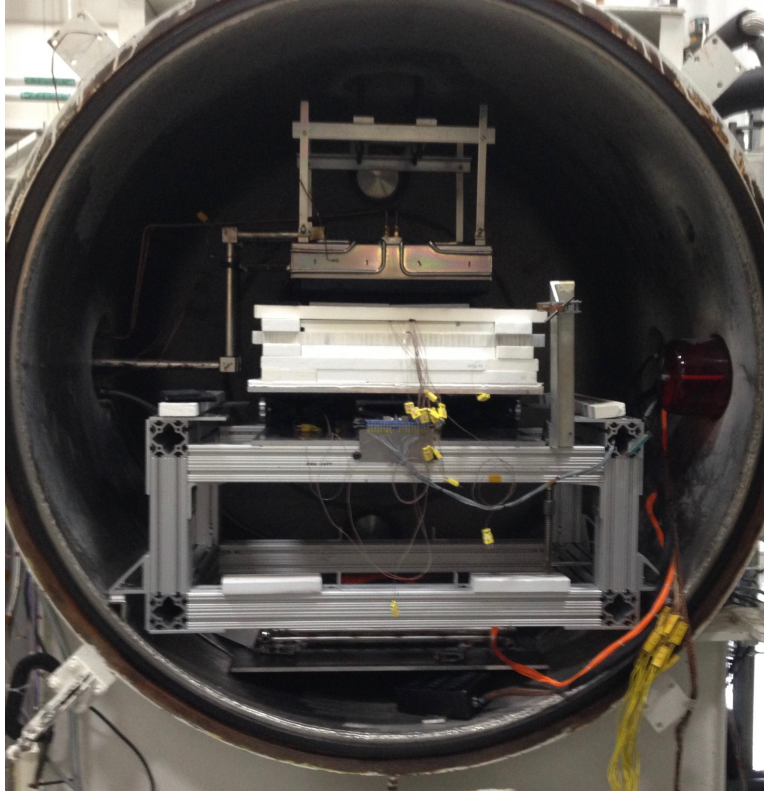
Figure 4.2: Testing Apparatus in Thermal Vacuum Chamber

Research Center in Hampton, Virginia. The apparatus, as seen in Figure 4.2, is contained in a thermal vacuum chamber to allow control of the pressure during testing. This setup replicates intense thermal loads for high temperature applications.

4.2.1   Thermocouples

Thermocouples (TCs) are used to measure the temperatures within the apparatus during testing. TCs are made of two dissimilar metals. Two junctions are made by fusing the metals together. If the two junctions are at different temperatures, an electromotive voltage is developed. The amount of this voltage is directly proportional to the difference in temperature between the two junctions. There were two different types of TCs used in this experiment, type K and type C. Type K TCs are accurate to approximately 1500 degrees Kelvin. Type C TCs are accurate to approximately 2600 degrees Kelvin. Foil and

wire TCs were used within the setup. A type K foil TC can be seen in Figure 4.3 and a wire type C TC in Figure 4.4.
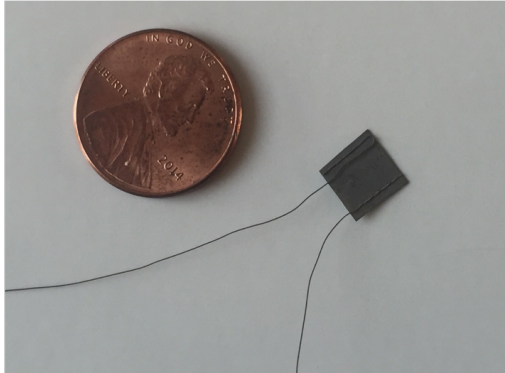
Figure 4.3: Type K Foil Thermocouple
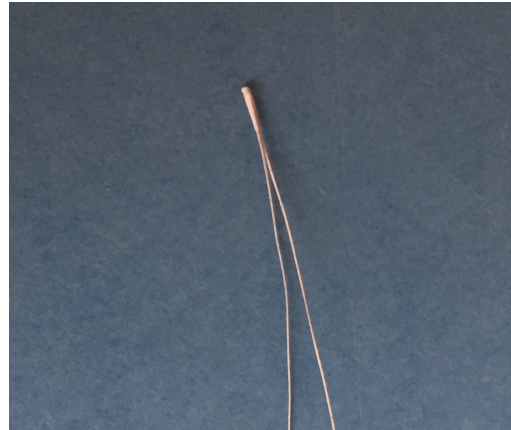
Figure 4.4: Type C Wire Thermocouple

4.2.2 Components of Setup

The lateral area of the set up is 12 inches by 12 inches. The heat is produced from a graphite heater at the top of the chamber. Directly below is a composite material, Advanced Carbon-Carbon 6 (ACC-6) plate. On this ACC-6 plate are eight embedded TCs. Four TCs are embedded on the top of the ACC-6 plate as seen in Figure 4.5 and four TCs are embedded on the bottom of the plate.

Below the ACC-6 plate are ten layers of APA seen in Figure 4.7. A diagram of the
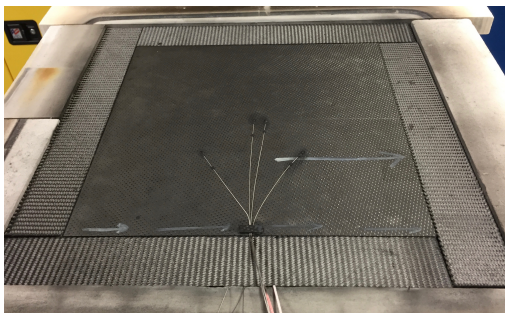
Figure 4.5: Top of Advanced Carbon-Carbon 6 Plate with 4 Embedded TCs
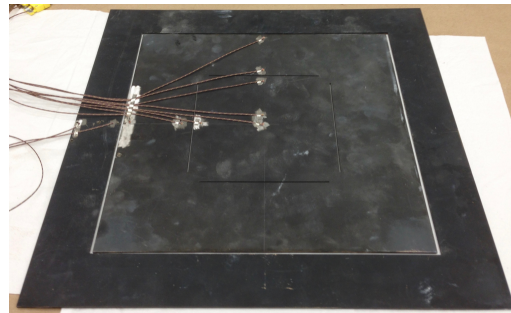
Figure 4.6: Bottom of Titanium Plate with 10 Embedded TCs

components in the setup can be seen in Figure 4.8. This insulation is used to verify the

Figure 4.7: Six Layers of Alumina Paper Insulation
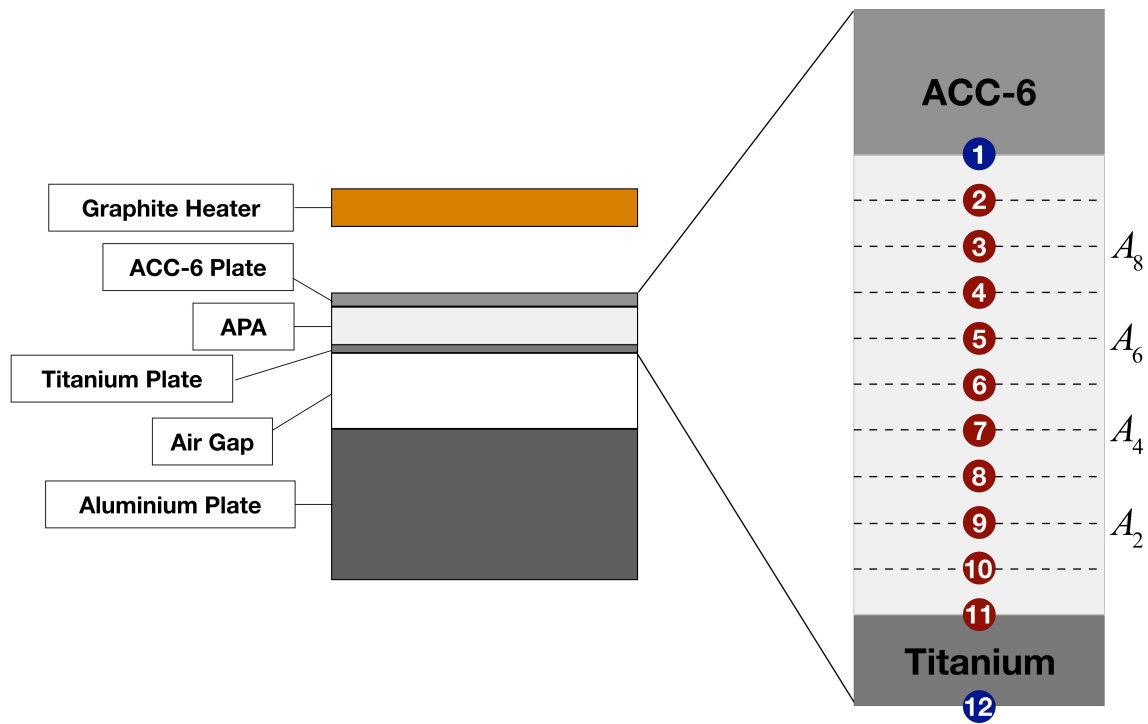
Figure 4.8: Experiment Diagram and Numerical Model

methodology as its thermal properties are known and validated. APA is produced in thin layers, approximately 0.05 inches thick. This allows for easy placement of TCs between layers. Within those ten layers of APA are four TCs. These TCs will be referenced as

A_2, A_4, A_6, A_8 where the subscript denotes the layer of APA they are on top of. For example, A_4 is placed on top of the fourth layer of APA when counting from the top of the titanium plate. These TC locations can be seen on the right of Figure 4.8. A_6 and A_8 are type C TCs since they see higher temperatures being located closer to the heat source. A_2 and A_4 are type K foil TCs as they do not see as high of temperatures. Below the APA insulation is a titanium plate as seen in Figure 4.6. On the titanium plate are ten embedded wire type K TCs; eight located centrally and two on the titanium picture frame. Below the titanium plate is a one inch air gap then a two inch thick aluminum plate that acts as a heat sink. This experiment was run at 100 Torr, 10 Torr, and 0.1 Torr. The Torr is a measurement of pressure and one Torr is equivalent to one millimeter of mercury. For comparison, one atmosphere is equal to 760 Torr. All three tests are similar in temperature profile but differ in test duration, max temperature, and initial temperature. This temperature data was used with the numerical model in the inverse heat transfer problem.

4.3   Numerical Model

In the simple one-dimensional numerical model, the domain modeled is from the bottom of the ACC-6 plate to the bottom of the titanium plate as seen on the right of Figure 4.8. It was assumed there is no thermal contact resistance between the flexible APA surrounding the rigid titanium and ACC-6 plates. The temperature data collected from the two center TCs on the bottom of the ACC-6 plate are averaged and used as the Dirichlet top, or hot side, boundary condition. This node is located at the interface of the insulation and ACC-6 plate as seen in Figure 4.8. The bottom boundary conditions or cold side boundary condition is the average of the four center TCs on the bottom of the titanium plate which corresponds to the bottom blue node in Figure 4.8. The initial condition, or initial temperature of the material was a linear interpolation of the initial temperature data

from the TCs used. A total of twelve nodes were used with nine of them in the insulation and one on the interface between the insulation and titanium plate, node 11, as seen in Figure 4.8.
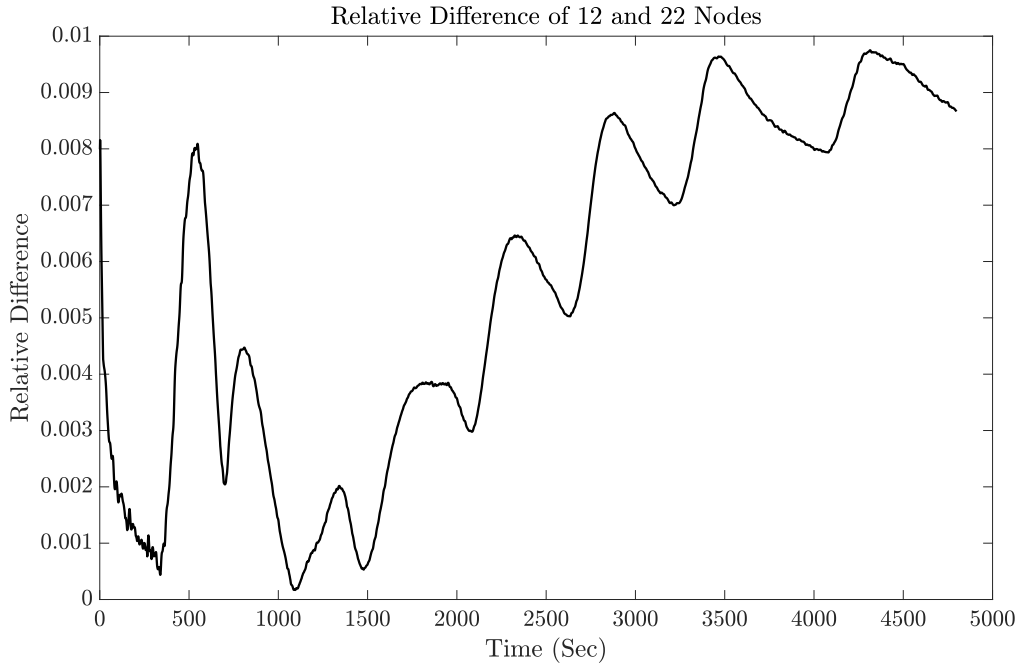
Figure 4.9: Relative Error of 12 Nodes and 22 Nodes

A nodal convergence study was completed to validate that twelve nodes was satisfactory in capturing the temperature gradient through the material. To do this, the direct model was run with 12 nodes and 22 nodes. The two models have 10 internal nodes in common and the relative difference between the temperatures computed at these common locations were found. These differences were then summed for each time step and the results are given in Figure 4.9. It can be seen that the relative error was within 1% for all 10 common nodal locations. This would yield an average relative difference of 0.1% per node. When using 22 nodes, the simulations would take approximately 8 hours each where as when using 12 nodes, the algorithm would terminate within 2 hours. Because the relative difference was significantly small and the reduction in number of nodes made a drastic

28

change in the computational time, it was decided to proceed with 12 nodes.

4.3.1   Heat Transfer Model Parameters

In the numerical model constructed to mimic the heat transfer through the insulation and titanium, parameters need to be defined in order to use the model to estimate the thermal conductivity of APA.

Titanium Thermal Properties

The material thermal properties, k and c_p, for the type of titanium used, Ti-8Al-1Mo-1V, which is composed of 8% aluminum, 1% molybdenum, 1% vanadium, and 90% titanium were inferred from data created by the Thermophysical Properties Research Lab (TPRL) [12]. Thermal conductivity and specific heat are third order polynomial curve fits to this data.

APA Specific Heat

Since the thermal conductivity of APA was estimated, only the specific heat was entered into the model. The APA used is composed of 86% alumina, 10% silica, and 4% other oxides. The specific heat used for this APA was theoretical data for alumina from [13].

4.3.2   CGA Parameters

In the CGA, as discussed in section 4.1, an initial population size of 40 was used with a mutation rate of 20 percent. For the search intervals of each coefficient, the maximum and minimum values used are the overall maximum and minimum values for that coefficient for all known fibrous insulations. These intervals are given below:

$$c_0 \in [-2.257 \times 10^{-2}, 2.017 \times 10^{-2}]$$

$$c_1 \in [-9.260 \times 10^{-5}, 1.279 \times 10^{-4}]$$

$$c_2 \in [-1.964 \times 10^{-7}, 1.470 \times 10^{-7}]$$

$$c_3 \in [3.351 \times 10^{-14}, 1.620 \times 10^{-10}]$$

After completing a run, the intervals were adjusted if the estimates were close to the boundary. The maximum number of iterations used was 300 with a tolerance of 0.01 for the objective value which yields an average temperature difference of less than 5 degrees Kelvin.

The methodology consists of all the combined steps and was applied to three tests at different pressures. Each TC location, A_2, A_4, A_6, and A_8 are used for comparison. Since the CGA creates the initial population at random, the code was executed three times per TC location to get variation in the estimates. The results are discussed in the next chapter.

Chapter 5

Results

In this chapter, the thermal conductivity estimates using the methodology discussed are presented and examined for various sets of data. Along with the thermal conductivity results, specific heat for one set of data is also shown. These estimates are compared to the known values of thermal conductivity and specific heat of APA and conclusions are drawn.

5.1   Thermal Conductivity Estimates

The results of the methodology to estimate the material thermal properties of APA using real temperature data are discussed. Data was collected from the testing apparatus at three different pressures: 100 Torr, 10 Torr, and 0.1 Torr. This data was preexisting and was not run for the specific task of estimating the material thermal properties of APA. It was important to apply this methodology to tests that were conducted at various pressures as thermal conductivity of a fibrous insulation such as APA varies with pressure. In higher pressures, the thermal conductivity of gas plays a bigger role than at lower pressures due to the presence of more gas molecules to transfer the heat. The results from the algorithm for each test are discussed. The estimate shown for each TC location is the result that produced the lowest cost, or objective function, value. The results of each test include

a table of the estimated coefficients for each TC location with a graph of the associated thermal conductivities for each. The current known values of thermal conductivity for APA are also plotted.

5.1.1   100 Torr Test
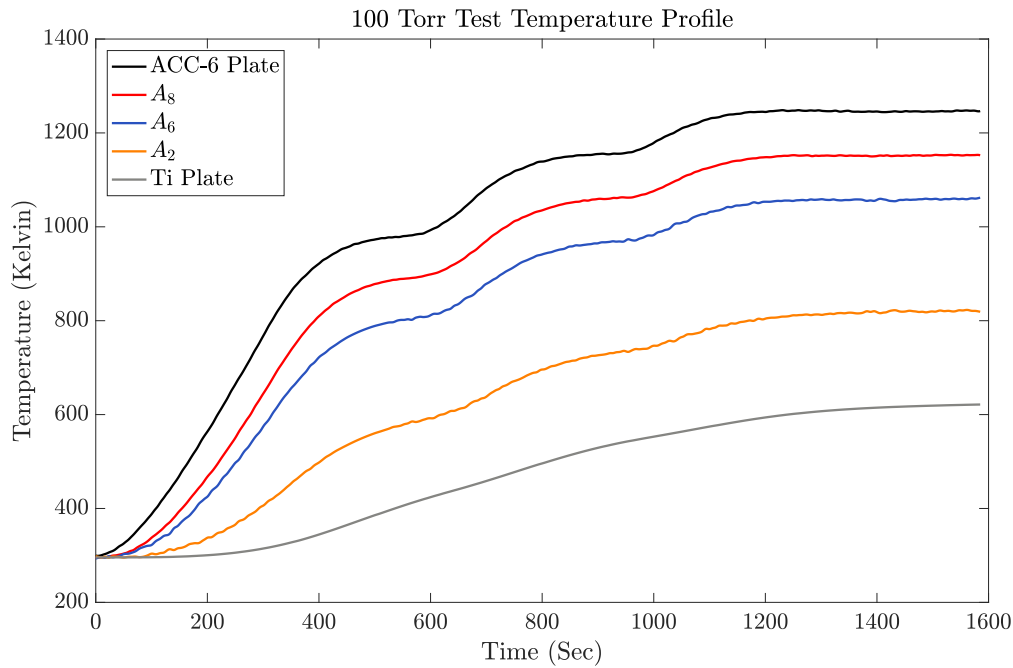
Figure 5.1: Temperature Profile of 100 Torr Test

Each test profile consisted of multiple ramps and dwells at various temperatures. For example, the temperature profile of the 100 Torr test, given in Figure 5.1, there were six ramps and dwells. The top black line is an average temperature of the two center TCs on the bottom of the ACC-6 plate. This specified temperature will be used as the top or hot side boundary condition. The bottom gray line corresponds to the average temperature of the four center TCs on the bottom of the titanium plate. This specified temperature is used as the bottom or cold side boundary condition in the numerical model.

32

This high pressure test was 1586 seconds in length and was the shortest test out of the three. This test reached a maximum temperature of approximately 1300 degrees Kelvin. The temperature profile can be seen in Figure 5.1. This test had three ramps and dwells, the least out of the three tests. The thermal conductivity coefficients with the lowest cost, or objective function, value received from each TC location are provided in Table 5.1. These coefficients are used in Equation 4.1 and the tabulated thermal conductivity values can be found in Table A.1 of the Appendix. The A_4 TC malfunctioned for this test, thus its values are not included. In Figure 5.2, the thermal conductivity cubic polynomial results for each TC location are given as well as the current known values of thermal conductivity of APA at 100 Torr.

TC Location	Cost	c_0	c_1	c_2	c_3
A_2	0.023	1.17×10^{-5}	1.01×10^{-4}	-5.89×10^{-8}	8.03×10^{-11}
A_4	N/A	N/A	N/A	N/A	N/A
A_6	0.077	7.31×10^{-8}	9.06×10^{-5}	-3.73×10^{-11}	9.96×10^{-12}
A_8	0.026	5.98×10^{-5}	4.99×10^{-5}	-8.50×10^{-9}	9.92×10^{-12}

Table 5.1: Thermal Conductivity Coefficients for 100 Torr Test

In Figure 5.2, it is evident that the estimate received from using the A_2 TC location matches best with the published thermal conductivity values. For the lower temperatures, the thermal conductivity is slightly over estimated. How the material will perform with higher temperatures is what is in question, thus this is not a large concern. Between 800 degrees Kelvin and 1100 degrees Kelvin, the estimates are not far off. Towards the high temperatures, between 1200 degrees Kelvin and 1400 degrees Kelvin, the methodology did an excellent job estimating the thermal conductivity of APA. Recall that this location was the furthest away from the heat source. The known values of thermal conductivity of APA at 100 Torr are given in the Appendix, Table A.1 [2]. These published values are known to be within 10% of real values and are even closer for higher temperatures. There is an average percent difference of 7.29%. The average percent difference for temperatures larger than 800 degrees Kelvin, is 2.72%.
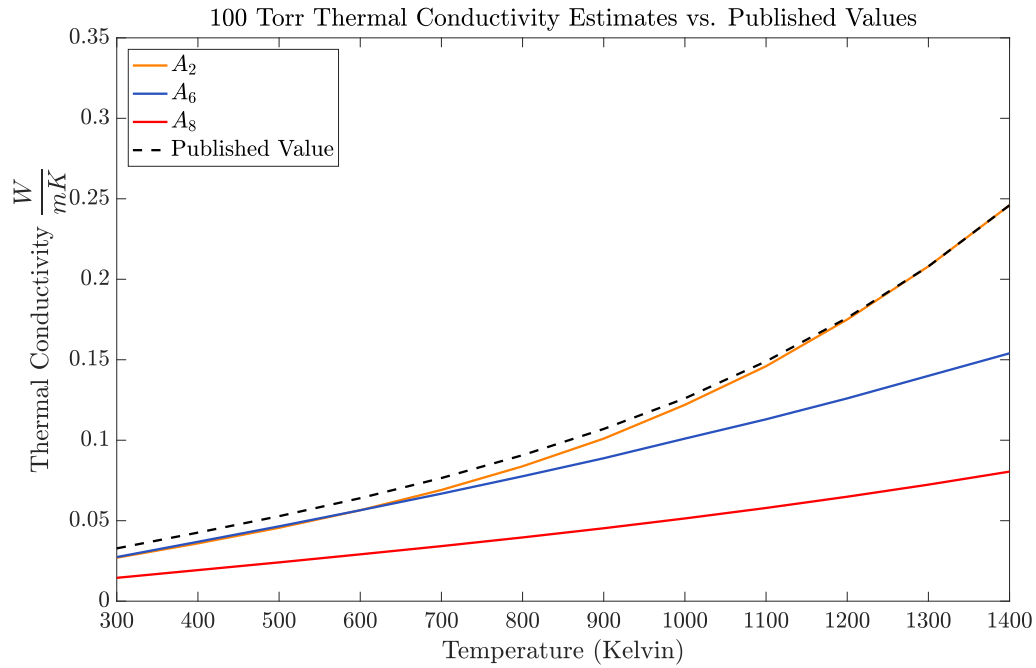
Figure 5.2: APA 100 Torr Thermal Conductivity Estimates vs Published Values

5.1.2   10 Torr Test

Figure 5.3: Temperature Profile of 10 Torr Test

The temperature profile can be seen in Figure 5.3. This test had five ramps and dwells and a maximum temperature of approximately 1550 degrees Kelvin. Also, this test had a duration of 4263 seconds and the associated thermal conductivity coefficients are given in Table 5.2. The tabulated thermal conductivity values are located in the appendix, Table A.2 and the results are graphed in Figure 5.4.

TC Location	Cost	c_0	c_1	c_2	c_3
A_2	0.010	6.87×10^{-4}	1.00×10^{-4}	-9.03×10^{-8}	9.68×10^{-11}
A_4	0.021	-8.42×10^{-3}	1.15×10^{-4}	-8.42×10^{-8}	7.22×10^{-11}
A_6	0.054	3.73×10^{-2}	1.93×10^{-7}	-2.00×10^{-9}	3.51×10^{-11}
A_8	0.067	2.50×10^{-2}	1.54×10^{-6}	-1.47×10^{-9}	1.70×10^{-11}

Table 5.2: Thermal Conductivity Coefficients for 10 Torr Test
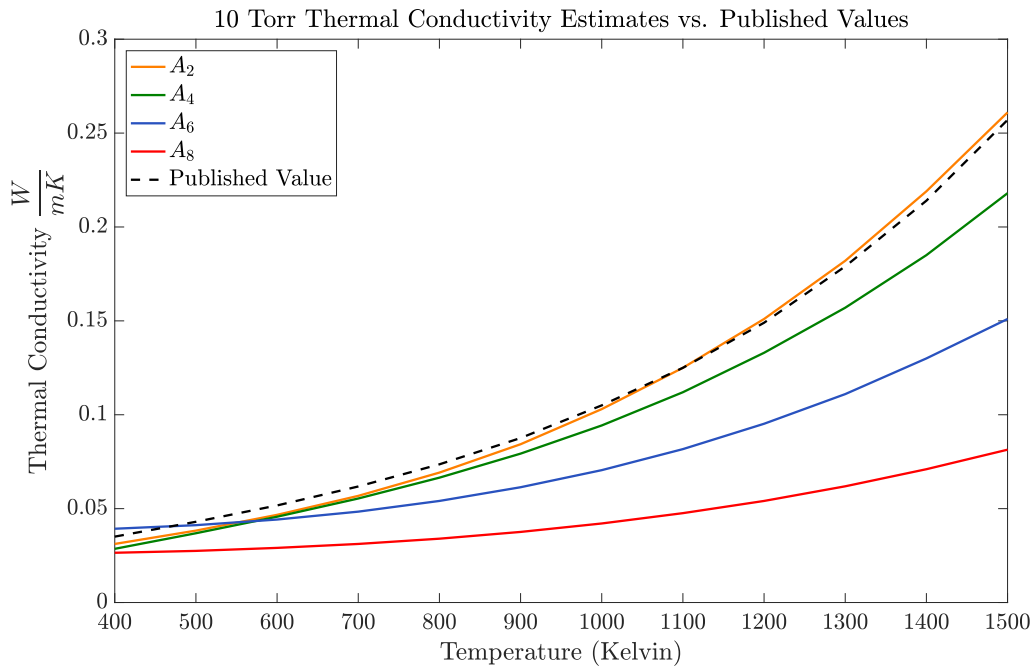
Figure 5.4: APA 10 Torr Thermal Conductivity Estimates vs Published Values

In Figure 5.4 it is shown again, the thermal conductivity polynomial using TC location A_2 gave the best estimate of thermal conductivity for APA at 10 Torr. These known values of thermal conductivity of APA at 10 Torr are given in the Appendix, Table A.2. In this graph, the average percent difference between the known values and the estimated values

35

are 5.45%. There is a larger difference at the lower temperatures, similarly to the previous results for the 100 Torr test. Toward the higher temperatures, the estimation is closer to the known values. From 800 degrees Kelvin to 1500 degrees Kelvin, the average percent difference between the estimated values using the A_2 TC location is 2.31%. This result further validated the methodology.
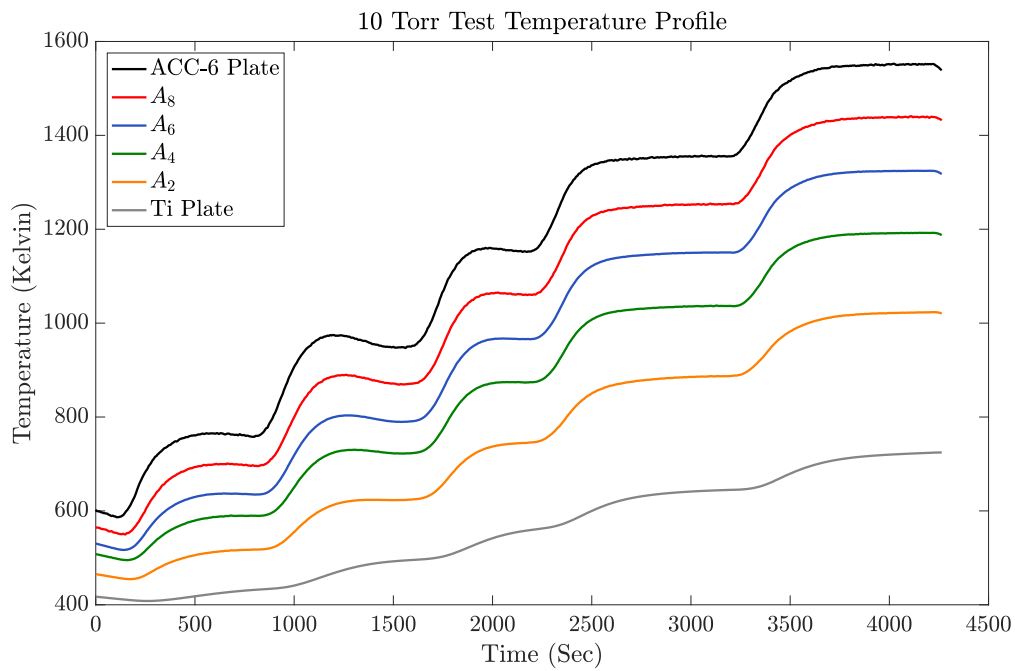
5.1.3   0.1 Torr Test
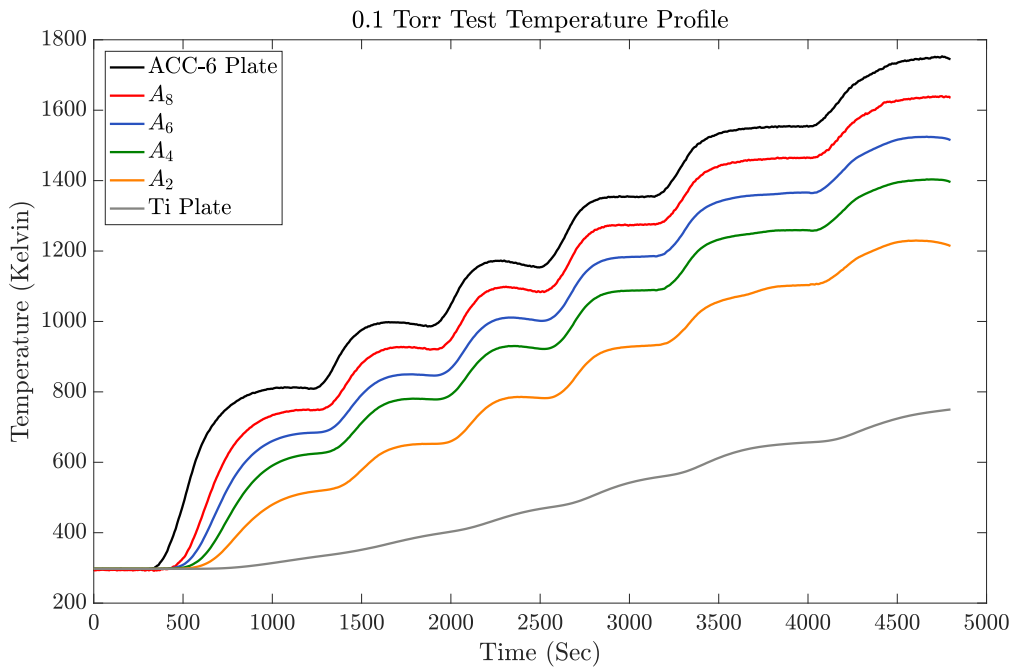
Figure 5.5: Temperature Profile of 0.1 Torr Test

The temperature profile can be seen in Figure 5.5. This test had six ramps and dwells and a maximum temperature of approximately 1750 degrees Kelvin. In Table 5.3 the coefficients and cost value from the objective function received when using the associated TC location are given. The tabulated thermal conductivity and the known values of thermal conductivity of APA at 0.1 Torr are given in Table A.3 in the Appendix. The results are plotted with the known values in Figure 5.6. In this figure, the estimate received from TC location A_4 gave the best result compared to the known values of thermal conductivity

of APA at 0.1 Torr. The average percent difference between the published values and the estimate at the A_4 TC location is 9.44% over the entire temperature range and 2.41% when above 800 degrees Kelvin.

TC Location	Cost	c_0	c_1	c_2	c_3
A_2	0.363	5.92×10^{-4}	2.60×10^{-5}	-5.92×10^{-8}	9.83×10^{-11}
A_4	0.067	3.16×10^{-3}	4.97×10^{-6}	-1.55×10^{-8}	6.76×10^{-11}
A_6	0.124	-1.89×10^{-3}	1.70×10^{-5}	-8.52×10^{-9}	3.26×10^{-11}
A_8	0.274	-5.88×10^{-3}	2.67×10^{-5}	-2.54×10^{-8}	3.06×10^{-11}

Table 5.3: Thermal Conductivity Coefficients for 0.1 Torr Test
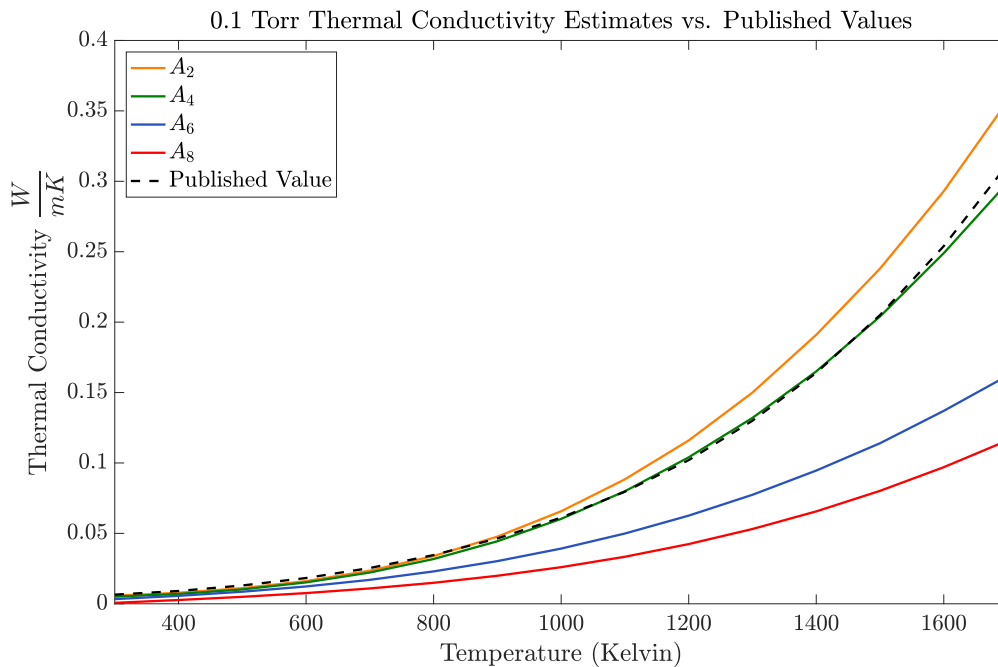
Figure 5.6: APA 0.1 Torr Thermal Conductivity Estimates vs Published Values

In all three sets of results, each TC location gave different estimates. Consistently, the TC location farthest away from the heat, A_2, gave the highest estimate of thermal conductivity. A_8 gave the lowest thermal conductivity estimate with A_4 and A_6 falling in between, respectively. In all cases, the TC locations farthest away from heat source, A_4 and A_2 gave the best approximations to the known, validated thermal conductivity values for

APA. It is possible that the other TC locations, A_6 and A_8, are not capturing the correct thermal conductivity as they are located closer to the heat source. These locations increase in temperature quickly, thus the thermal conductivity could not be well estimated because of this quick rise. It was seen in the 100 and 10 Torr test that the thermal conductivity was best estimated by TC location A_2. However, in the 0.1 Torr Test the A_4 TC location gave the best approximation. This could be because in low pressures, the heat transfer is slower than in higher pressures and TC location A_2 does not increase in temperature as dramatically in the lower pressure, 0.1 Torr, than in the other higher pressures, 10 and 100 Torr.

In all three sets of thermal conductivity results for 100, 10, and, 0.1 Torr, it was seen that cost values for various TC locations were often close in value. For example, in the results for thermal conductivity at 0.1 Torr, TC location A_8 gave a cost value of 0.274 where as the thermal conductivity from TC location A_2 gave a cost value of 0.363. It is seen in Figure 5.6 that the thermal conductivity received from the A_2 TC location was closer to the published values than the estimate from TC location A_8 but A_8 had a lower cost value. To better understand why this was occurring, the thermal conductivity from each location at 0.1 Torr was used in the direct model and temperature data was computed. The absolute difference between the computed model data using the four different sets of temperature and collected experimental data at each TC location was then calculated. The plots can be seen below in Figure 5.7.

The total temperature differences using the thermal conductivity estimate from TC A_8 are approximately 25 degrees where as the temperature differences from TC A_2 are approximately 15 degrees.
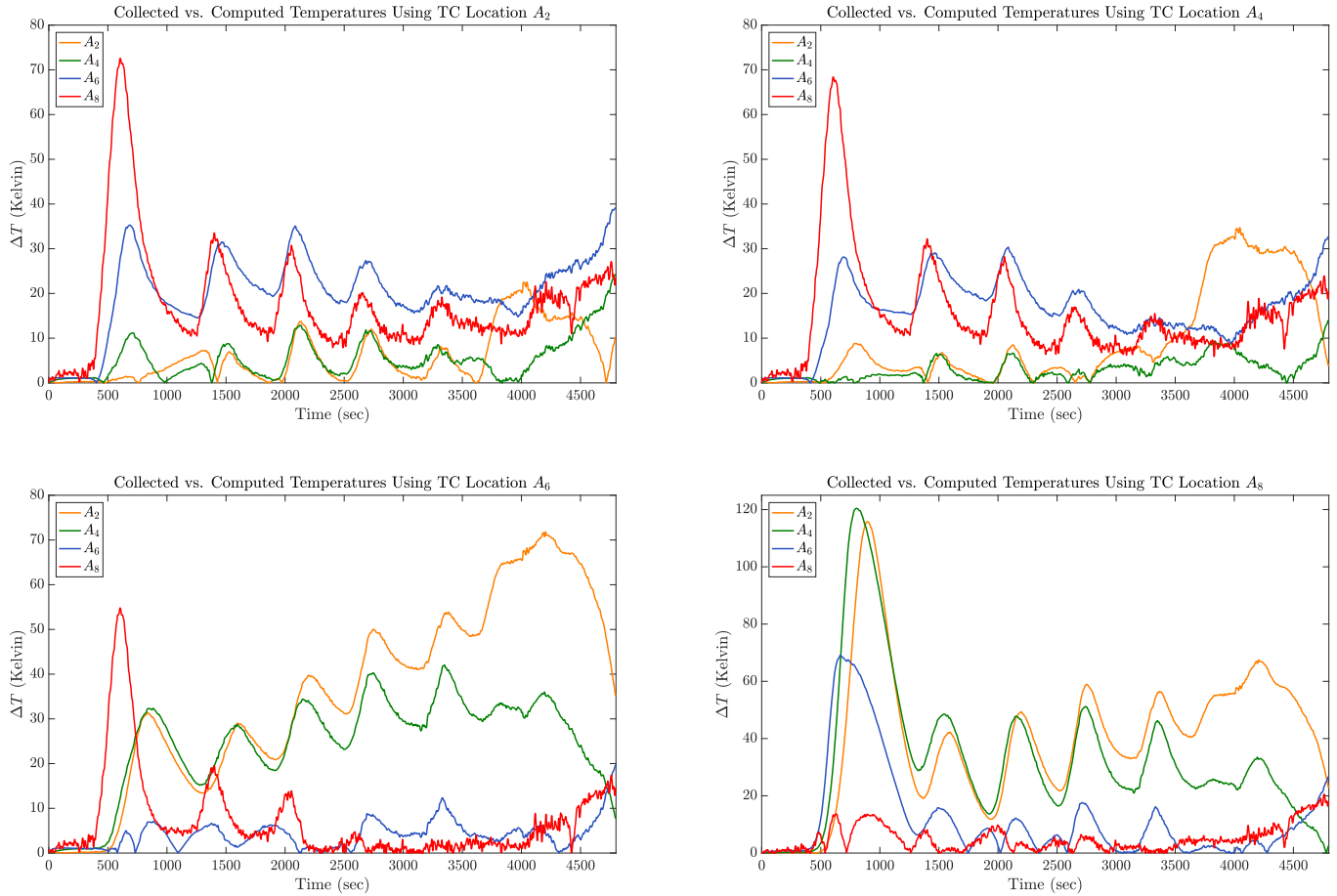
Figure 5.7: Difference of Collected vs. Computed Temperatures at 0.1 Torr

5.2   Sensitivity Analysis

To understand why the lower TCs were giving the best approximation, the sensitivity of thermal conductivity with respect to location was found. The partial derivative of thermal conductivity , k, with respect to location, x, was found.

$$\frac{\partial k}{\partial x} = \frac{\partial k}{\partial T} \cdot \frac{\partial T}{\partial x} \approx \left(c_1 + 2c_2 T(x) + 3c_3 T(x)^2 \right) \left(\frac{T(x + \Delta x) - T(x)}{\Delta x} \right)$$

 In Figure 5.8 is a plot of the sensitivity of thermal conductivity with respect to position for each TC location using the 10 Torr test data. It can be seen that during the first few temperature rises, the TC closest to the heat is the most sensitive. During the dwells at the

39
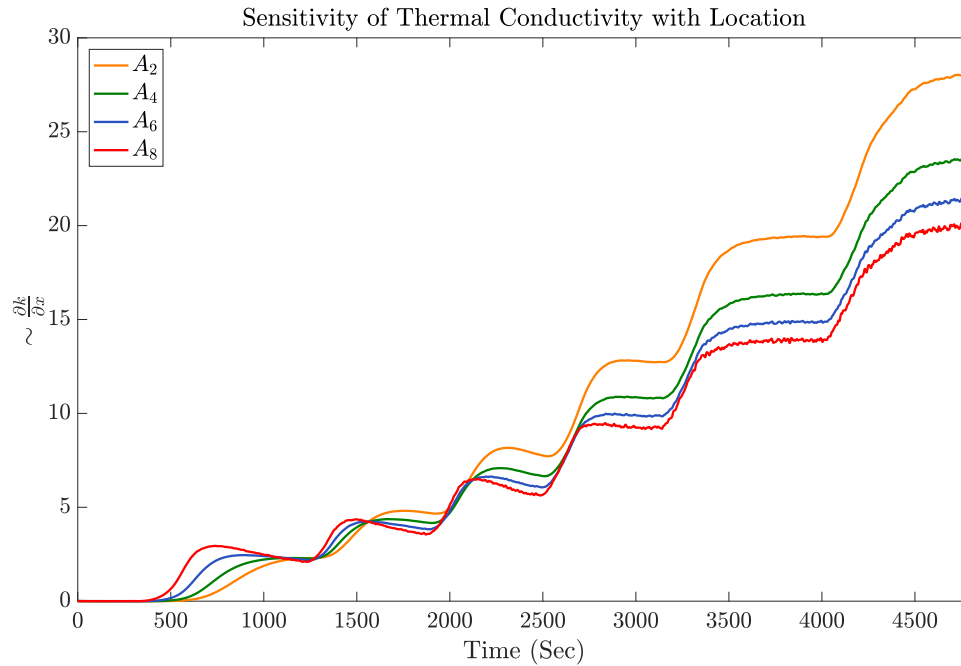
Figure 5.8: Sensitivity of Thermal Conductivity with Location for 0.1 Torr Test

lower temperatures, the sensitivities are very similar but as the temperature increases, the TC locations farther away from the heat have the greatest sensitivity. This could be why these locations gave the best approximations.

In Figure 5.9, all thermal conductivity estimates are plotted with the published values. In this figure, it is shown how thermal conductivity can vary with pressure as well as, how accurately the method estimated the thermal conductivity of APA for the three pressures 0.1, 10, and 100 Torr. All estimates are within 10% of the published values.

5.3   Specific Heat Results

This methodology was applied to the 100 Torr temperature data discussed in the previous section to estimate specific heat. The estimation of this material thermal property was applied only to this test as there is more confidence of estimating specific heat for fibrous insulation using the standard method discussed in Chapter 2. Similarly to estimating
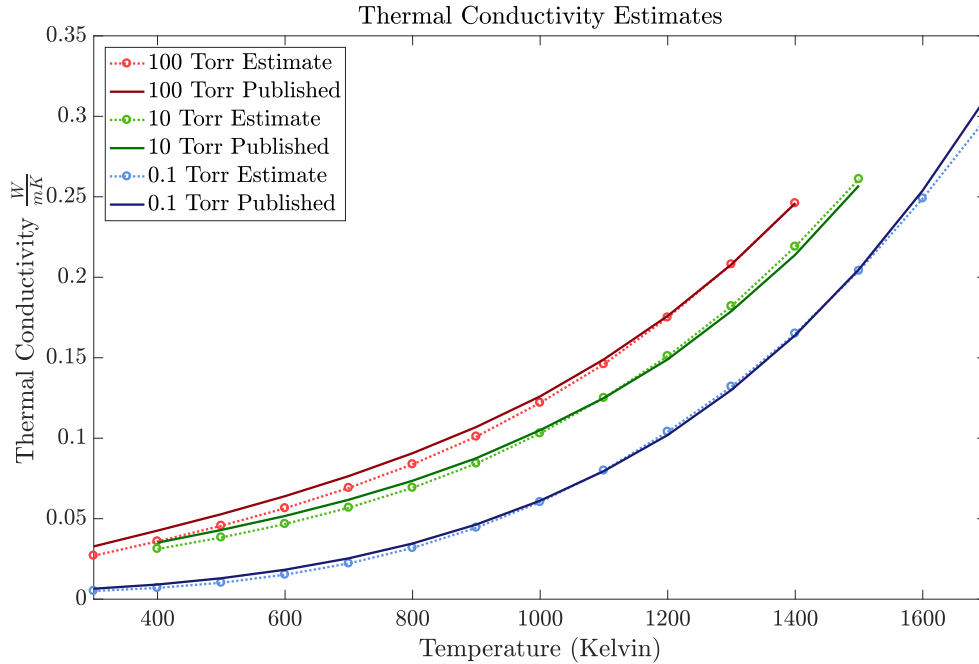
Figure 5.9: All Thermal Conductivity Estimates vs. Published Values

thermal conductivity where specific heat was assumed to be known, here the thermal conductivity was assumed to be known so specific heat could be estimated. To estimate specific heat, the functional form assumed is given in Equation 5.1.

$$c_p(T) = b_0\Big(1 - \frac{1}{e^{b_1 T}}\Big) \tag{5.1}$$

This functional form is similar to the functional form used in [14] for the specific heat capacity of Alumina. It is likely that a general cubic polynomial will be satisfactory; however, estimating the functional form of 5.1 reduces the number of parameters estimated by two. In Table 5.4, the coefficients and associated cost value from each TC location are given.

These results are graphed in Figure 5.10 and the tabulated specific heat estimates and known values are given in Table A.4 in the appendix. It is seen in Figure 5.10 that again, TC location A_2 produced the most accurate estimate. The A_8 TC location extremely

41

TC Location	Cost	b_0	b_1
A_2	0.021	1.34×10^3	2.81×10^{-3}
A_4	N/A	N/A	N/A
A_6	0.211	1.91×10^3	1.81×10^{-3}
A_8	0.123	6.06×10^3	8.09×10^{-4}

Table 5.4: Specific Heat Coefficients for 100 Torr Test
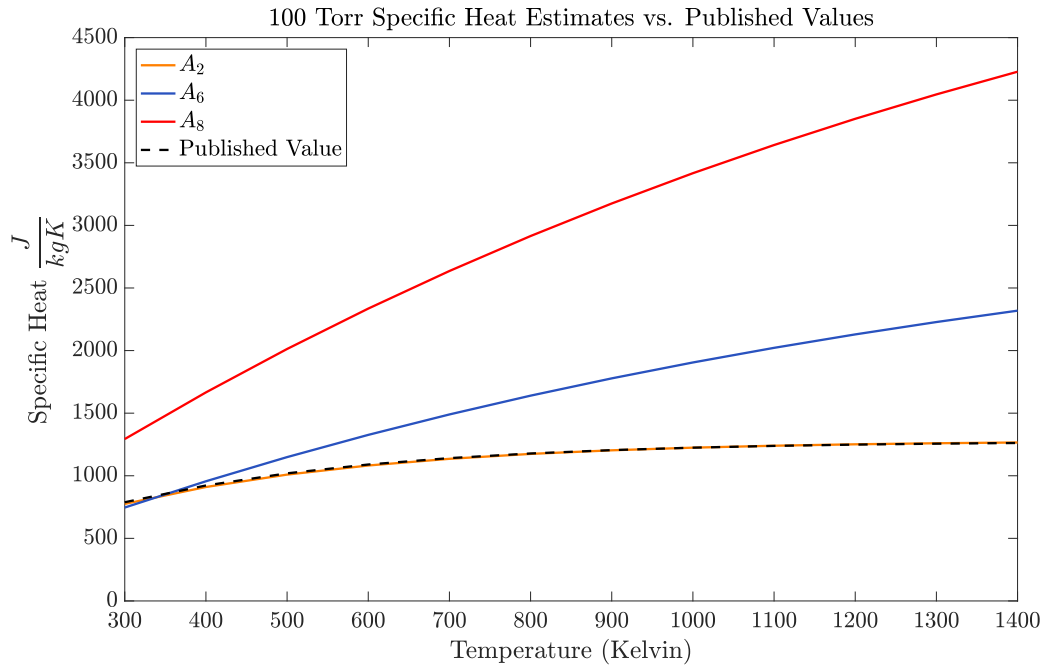
Figure 5.10: APA 100 Torr Specific Heat Estimates vs Published Values

overestimated the actual specific heat values. The average percent difference of the approximated and known values is 2.47%.

Chapter 6

Concluding Remarks and Future Research

In this work, material thermal properties of a fibrous insulation, APA, were estimated. This was done using the transient thermal testing apparatus at NASA Langley Research Center to collect temperature data within the insulation while it is exposed to extreme temperatures. A one-dimensional numerical model was built to replicate the heat transfer within the apparatus. The difference between the test data and computed values were minimized by estimating the coefficients of thermal conductivity as a third order polynomial. This was done using the CGA to estimate those coefficients. The application background, methodology, and experiment apparatus was discussed.

6.1   Conclusions

A combination of the transient thermal testing apparatus at NASA Langley Research Center, one-dimensional numerical modeling, and the CGA was successful in estimating material thermal properties of APA. It was seen that the estimates varied with location within the material. It was found that the TC locations farthest away from the heat, A_2

and A_4, gave the best approximations. For the 100 Torr and 10 Torr tests, A_2 accurately estimated the thermal conductivity of APA at those pressures. For the 100 Torr test, the estimate from the A_2 TC location produced an average percent difference of 7.29% for the entire temperature range and an average percent difference of 2.72% when above 800 degrees Kelvin. For the 10 Torr test, the estimate from the A_2 TC location produced an average percent difference of 5.45% for the entire temperature range and an average percent difference of 2.31% when above 800 degrees Kelvin. For the 0.1 Torr test, the A_4 location was the most successful estimate of the thermal conductivity values. This location gave an average percent difference of 9.44% over the entire temperature range and an average percent difference of 2.49% when above 800 degrees Kelvin. Location of A_4 giving the best approximation for the 0.1 Torr test could be due to the low pressure of the test and how it affects the rate of heat transfer. Specific heat was also estimated using this technique. TC location A_2 gave the best approximation with an average percent difference of 2.47% over the entire temperature range.

This methodology allowed for thermal conductivity results for a large temperature range using only one set of transient temperature data. It was found that the locations farther away from the heat source, A_2 and A_4, gave the best estimates. This was validated for three tests at three various pressures for thermal conductivity and one test for specific heat.

6.2   Future Research

Future research will include further validating this methodology, by applying various test setups and insulations. The transient temperature data used was not originally collected to perform this research. The profiles of the data used for this work consisted of many ramps and dwells. It is of interest to see if a change in the profile of the temperature

44

data used would change the convergence rate of the algorithm. If the testing length was significantly decreased and the profile was changed to a constant, single ramp rate to produce a smooth curve, the computational time could be reduced.

Thermal conductivity and specific heat were estimated separately, instead it is of interest to investigate if these two properties can be estimated simultaneously using this same methodology. Also of interest is the location within the material that gives the most accurate estimate. In the results, it was seen that the estimates for various locations were different. In particular, the locations at the bottom of the insulation, away from the heat source, were most successful in approximating the material thermal properties. This opens up the question, is there a particular location within the test setup that would produce the best estimates of thermal conductivity? To explore this, additional TCs can be placed within the material to better understand the variability of estimation with location.

The material of interest for this research was a fibrous insulation. Not all insulations are made of fibers. Attempting to apply this methodology to other types of insulations that are not fibrous would be of interest.

Material thermal properties of a fibrous insulation, APA, were estimated using transient temperature data with numerical heat transfer modeling and the Continuous genetic algorithm. The results validated the methodology and gave confidence in applying this method to other materials and temperature data in the future.

45

Bibliography

[1] Çengel, Y. and Ghajar, A., *Heat and Mass Transfer: Fundamentals & Applications*, McGraw-Hill, New York, 2011.

[2] Daryabeigi, K., Cunnington, G. R., Miller, S. D., and Knutson, J. R., "Combined Heat Transfer in High-Porosity High-Temperature Fibrous Insulation: Theory and Experimental Validation," *International Journal of Thermophysics*, Vol. 25, No. 4, October–December 2011, pp. 536-546.

[3] ASTM C177-13, Standard Test Method for Steady-State Heat Flux Measurements and Thermal Transmission Properties by Means of the Guarded-Hot-Plate Apparatus, ASTM International, West Conshohocken, PA, 2013, www.astm.org

[4] ASTM C518-17, Standard Test Method for Steady-State Thermal Transmission Properties by Means of the Heat Flow Meter Apparatus, ASTM International, West Conshohocken, PA, 2017, www.astm.org

[5] Gembarovic, J. and Taylor, R. E., "A Method for Thermal Diffusivity Determination of Thermal Insulators," *International Journal of Thermophysics*, Vol. 28, No. 6, 2007, pp. 2164-2175.

[6] ASTM E1269-11, Standard Test Method for Determining Specific Heat Capacity by Differential Scanning Calorimetry, ASTM International, West Conshohocken, PA, 2011, www.astm.org

[7] Czél, B., and Gróf, G., "Genetic Algorithm-Based Method for Determination of Temperature-Dependent Thermophysical Properties," *International Journal of Thermophysics*, Vol. 30, No. 6, 2009, pp. 1974-1991.

[8] Bradie, B., *A Friendly Introduction to Numerical Analysis*, Pearson Prentice Hall, Upper Saddle River, 2006.

[9] Thomas, L. H., "Elliptic Problems in Linear Differential Equations over a Network," Watson Sci. Comput. Lab Report, New York, 1949.

[10] Özisik, M. and Orlande, H. R. B., *Inverse Heat Transfer: Fundamentals and Applications*, CRC Press, Boca Raton, 2000.

[11] Haupt, R. L. and Haupt, S. E., *Practical Genetic Algorithms*, Wiley, Hoboken, 1998.

[12] Thermophysical Properties Research Lab, "Thermophysical Properties of Ti-8-1-1 Alloy," (Report #4677)., March, 2011.

[13] Touloukian, Y. S. and Buyco, E. H., *Thermophysical Properties of Matter. Volume 5. Specific Heat-Nonmetallic Solids*, IFI/Plenum, New York, 1970.

[14] de Faoite, D., Browne, D. J., and Stanton, K. T.,"Regression analysis of temperature-dependent mechanical and thermal properties of dielectric technical ceramics," *Journal of Materials Science*, 2013, Vol. 48, No. 1, pp.451-461.

47

Appendix A

Tables of Estimated Thermal Conductivity and Specific Heat Values of Alumina Paper

Temperature (Kelvin)	A_2	A_4	A_6	A_8	Published Values [2]
300	2.70E-02	N/A	2.74E-02	1.45E-02	3.28E-02
400	3.59E-02	N/A	3.69E-02	1.93E-02	4.26E-02
500	4.56E-02	N/A	4.65E-02	2.41E-02	5.28E-02
600	5.65E-02	N/A	5.65E-02	2.91E-02	6.40E-02
700	6.91E-02	N/A	6.68E-02	3.42E-02	7.65E-02
800	8.38E-02	N/A	7.76E-02	3.96E-02	9.07E-02
900	1.01E-01	N/A	8.88E-02	4.53E-02	1.07E-01
1000	1.22E-01	N/A	1.01E-01	5.14E-02	1.26E-01
1100	1.46E-01	N/A	1.13E-01	5.79E-02	1.49E-01
1200	1.75E-01	N/A	1.26E-01	6.49E-02	1.76E-01
1300	2.08E-01	N/A	1.40E-01	7.24E-02	2.08E-01
1400	2.46E-01	N/A	1.54E-01	8.05E-02	2.46E-01

Table A.1: Thermal Conductivity Estimates at 100 Torr

Temperature (Kelvin)	A_2	A_4	A_6	A_8	Published Values [2]
400	3.12E-02	2.86E-02	3.93E-02	2.65E-02	3.51E-02
500	3.83E-02	3.69E-02	4.12E-02	2.75E-02	4.30E-02
600	4.67E-02	4.57E-02	4.42E-02	2.91E-02	5.17E-02
700	5.68E-02	5.54E-02	4.84E-02	3.12E-02	6.18E-02
800	6.92E-02	6.65E-02	5.41E-02	3.40E-02	7.36E-02
900	8.43E-02	7.93E-02	6.14E-02	3.76E-02	8.76E-02
1000	1.03E-01	9.43E-02	7.05E-02	4.21E-02	1.05E-01
1100	1.25E-01	1.12E-01	8.17E-02	4.76E-02	1.25E-01
1200	1.51E-01	1.33E-01	9.52E-02	5.41E-02	1.49E-01
1300	1.82E-01	1.57E-01	1.11E-01	6.19E-02	1.79E-01
1400	2.19E-01	1.85E-01	1.30E-01	7.10E-02	2.14E-01
1500	2.61E-01	2.18E-01	1.51E-01	8.14E-02	2.57E-01

Table A.2: Thermal Conductivity Estimates at 10 Torr

Temperature (Kelvin)	A_2	A_4	A_6	A_8	Published Values [2]
300	5.73E-03	5.08E-03	3.33E-03	6.68E-04	6.50E-03
400	7.83E-03	6.99E-03	5.65E-03	2.69E-03	9.10E-03
500	1.11E-02	1.02E-02	8.57E-03	4.94E-03	1.30E-02
600	1.61E-02	1.52E-02	1.23E-02	7.60E-03	1.83E-02
700	2.35E-02	2.22E-02	1.70E-02	1.09E-02	2.54E-02
800	3.39E-02	3.18E-02	2.30E-02	1.49E-02	3.46E-02
900	4.77E-02	4.44E-02	3.03E-02	1.99E-02	4.64E-02
1000	6.57E-02	6.03E-02	3.92E-02	2.60E-02	6.12E-02
1100	8.84E-02	7.99E-02	4.99E-02	3.34E-02	7.96E-02
1200	1.16E-01	1.04E-01	6.26E-02	4.24E-02	1.02E-01
1300	1.50E-01	1.32E-01	7.74E-02	5.31E-02	1.30E-01
1400	1.91E-01	1.65E-01	9.46E-02	6.56E-02	1.64E-01
1500	2.38E-01	2.04E-01	1.14E-01	8.02E-02	2.05E-01
1600	2.93E-01	2.49E-01	1.37E-01	9.70E-02	2.54E-01
1700	3.57E-01	2.99E-01	1.62E-01	1.16E-01	3.12E-01

Table A.3: Thermal Conductivity Estimates at 0.1 Torr

49

Temperature (Kelvin)	A_2	A_4	A_6	A_8	Published Values
300	775.22811	N/A	746.134458	1293.34484	788.599843
400	910.163424	N/A	956.005254	1665.98749	922.357872
500	1009.22259	N/A	1149.01858	2012.73832	1019.40846
600	1081.94423	N/A	1326.52847	2335.39633	1089.8253
700	1135.33089	N/A	1489.78021	2635.63554	1140.91753
800	1174.52327	N/A	1639.91907	2915.01364	1177.98844
900	1203.29532	N/A	1777.99831	3174.98009	1204.88591
1000	1224.41755	N/A	1904.9866	3416.88364	1224.40187
1100	1239.92388	N/A	2021.77479	3641.97935	1238.56203
1200	1251.30743	N/A	2129.18219	3851.43503	1248.83619
1300	1259.66436	N/A	2227.9623	4046.33739	1256.2908
1400	1265.79938	N/A	2318.80808	4227.69762	1261.69963

Table A.4: Specific Heat Estimates at 100 Torr

50

Vita

Elora Frye is from Yorktown, Virginia. She graduated from Grafton High School in 2012. From there she attended Virginia Commonwealth University in Richmond, Virginia where she obtained a Bachelor of Science in mathematics with a concentration in applied mathematics. She is currently a candidate for a Master of Science in applied mathematics also at Virginia Commonwealth University.